# Supramolecular Structure and Dynamics of Organic Molecules Adsorbed on the External Surface of MFI Zeolites. A Direct and Indirect Computational EPR Analysis

**M. Francesca Ottaviani,*,† Xue-gong Lei,‡ Zhiqiang Liu,‡ and Nicholas J. Turro*,‡**

*Institute of Chemical Sciences, University of Urbino, 61029 Urbino, Italy, and Department of Chemistry, Columbia University, New York, New York 10027*

*Received: March 26, 2001*

The nitroxides **1** and **1**-oMe were employed as EPR probes for the investigation of the supramolecular structures and dynamics of organic molecules adsorbed on the external surfaces of two MFI zeolites (silicalite and ZSM-5). The results for the two zeolites are qualitatively similar, but depend quantitatively on the surface area of the external surface. Computational analysis of the EPR spectra as a function of loading of the probe is consistent with an initial strong association of the probes with the holes on the external surface, followed by a weaker binding to the framework of the external surface between the holes. The first supramolecular structure (binding to holes) fixes the motion of the probes and allows for an estimation of the average separation of the probes through EPR analysis of the dipole−dipole interaction. After saturation of the holes and the onset of the second supermolecular structure (binding to the framework), rapid diffusion of the probes on the framework occurs and provides a means for an estimation of the motion of the probe through EPR analysis of the spin−spin exchange interaction. The mobile framework's probes collide and displace the probes in the holes, resulting in a dynamic equilibrium between probes at both sites. The displacement of the nitroxides associated with the holes by three coadsorbed "displacer" molecules, **2**, **3**, and **4**, was investigated by the change of the probe EPR. Addition of ketones **2** and **4** resulted in the displacement of nitroxides after sufficient displacer was added to saturate the holes on the external surface. This result is consistent with a stronger binding of the nitroxide to the surface and for the need for molecules of **2** and **4** to be situated on the framework before displacement of the nitroxide can occur. Compared to **2** and **4**, **3** is found to be a poor displacer of nitroxide because of its weak association with the holes. From the competitive displacements, it is concluded that the binding to the external surface increases in the series **3** < **2** < **4** ≪ **1**, being at a minimum for the nonpolar **3** and a maximum for the nitroxide that possesses two polar moieties for interaction with the zeolite surface. On the basis of these results, a model was developed which described the supramolecular structures and dynamics formed by the ketones and MFI zeolites at a function of loading and for the various systems investigated.

## Introduction

The MFI zeolites are important materials with applications in the catalytic and separation sciences.[1] The building blocks of MFI zeolites are the corner-sharing $AlO_2^-$ (with charge compensating cations) and $SiO_2$ tetrahedra with Al and/or Si atoms connected through oxygen atoms. These structural units create two sets of channel systems, one straight running along the direction of [010] and roughly circular with a diameter of ca. 5.3 × 5.6 Å and the other sinusoidal, running along the direction of [100] and roughly elliptical with dimensions of ca. 5.1 Å × 5.5 Å (Chart 1).[2] The channels and intersections compose the internal surface and the holes (pore openings), respectively, while the framework between the holes composes the external surface (Chart 1). Applications of zeolites typically begin with the initial size/shape selective adsorption of molecules (from the gas phase or the liquid phase) to the external surface of a zeolite crystal followed by size−shape selective diffusion and molecular sieving of the molecules to the internal surface.[3] Among the important and fascinating issues concerning the adsorption of molecules on the external surface to be examined are (1) What are the distinct supramolecular structures formed on the external surface? (2) Which (if any) supramo-

**CHART 1: Structure of MFI Zeolite**[a]

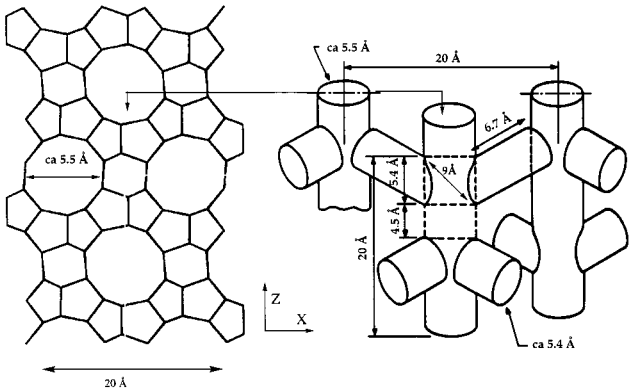


[a] Left, the projection of MFI zeolite along [010], showing the external surface consisting of Holes (pore openings) and framework between the holes. Right, the internal surface of MFI zeolite, consisting of straight channel along [010] direction and sinusoidal channel along [100] direction.

* Authors to whom correspondence should be addressed.
† University of Urbino.
‡ Columbia University.

10.1021/jp011110a CCC: $20.00 
Published on Web 07/24/2001

lecular structures are associated with the holes on the external surface, and which (if any) are associated with the external framework between the holes? (3) What are the relative binding strengths of systematically varied supramolecular structures of the sites on the external surface? (4) What are the dynamics of the molecules adsorbed at the sites on the external surface and of the displacement of initially bound molecules by other molecules that compete for sites? Such questions regarding adsorption and dynamics of molecules on zeolites can often be answered by spectroscopic methods.[4] However, despite its interest and importance, the literature on the use of spectroscopic methods to investigate the supramolecular structure and dynamics of molecules *adsorbed on the external surface* of zeolites is limited.[5] The relatively small surface area usually associated with the external surface and corresponding sensitivity issues probably contribute to the relative dearth of spectroscopic reports of the supramolecular structure and dynamics of molecules adsorbed on the external surface of zeolites.

In this report we demonstrate that electron paramagnetic resonance (EPR) provides a spectroscopic method of high sensitivity that is applicable for investigations of the supramolecular structure and dynamics of molecules bound to the external surface of MFI zeolites. The strategy for the investigation is derived from previous results that examined the photochemistry of dibenzyl ketone derivatives which were selectively adsorbed on the external surface of MFI zeolites.[5a,b] These studies concluded that there are two distinct binding sites on the external surface of MFI zeolites, i.e., an initial and stronger binding site that is associated with the holes, and the second, weaker binding site that is associated with the framework surface between the holes. Furthermore, it was shown that the stronger binding site (associated with the holes) constitutes ca. 30% of the external surface and the weaker binding site (associated with the framework) constitutes ca. 70% of the external surface.[5a] This model is consistent with X-ray data for the unit cell of MFI zeolites.[2] Chart 1 shows the external surface of a MFI crystal as a projection of the zeolite framework along the [010] direction. For a MFI sample with an external surface area of 10 $m^2/g$ (which is of the order of the zeolites employed in this investigation) the stronger binding sites are saturated at ca. 0.3 wt %/wt and a monolayer is formed at ca. 0.7 wt %/wt loading for an adsorbed molecule of molecular weight of 210 (e.g., dibenzyl ketone) taking an average of the limiting orientations of adsorbed molecules on the external surface.[5a]

On the basis of this working model we designed two nitroxide EPR probes (**1** and **1**-oMe, Chart 2) of the external surface of MFI zeolites to possess a partial structure that was analogous to the previously investigated dibenzyl ketones.[5a,d] The experimental approach envisioned was first to investigate the loading dependence of EPR of **1** and **1**-oMe adsorbed on the external surface of two MFI zeolites, silicalite and ZSM-5. These investigations examine the binding of the nitroxide probe to the various sites on the external surface as a function of the type of zeolite (silicalite vs ZSM-5) and the sensitivity of the binding to the structure of the guest. A second study was undertaken to investigate the displacement of the initially adsorbed nitroxide probes by the addition of molecules **2**, **3**, and **4**, (Chart 2) each of which possesses differing size/shape characteristics and functional groups.

**CHART 2: Structures of Molecules Investigated in This Report.**

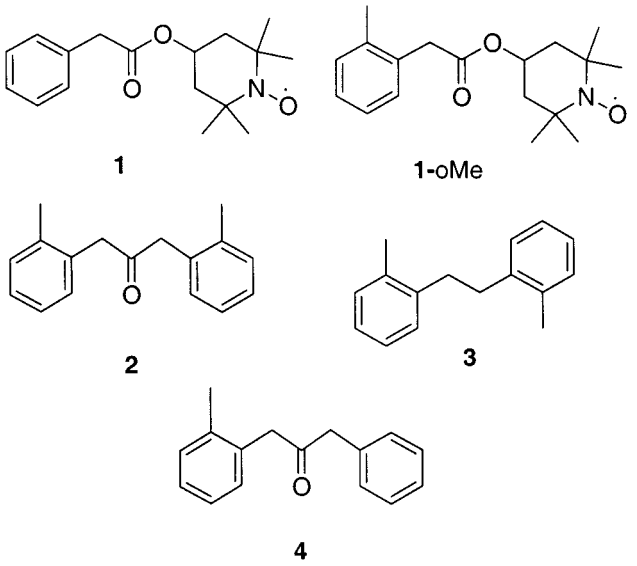


## Experimental Section

**General Methods.** All reagents were purchased from Aldrich and used as received, unless otherwise stated. Silica gel (EM Science, 230−400 mesh) was used for column chromatography. NMR spectra were recorded on a Bruker NMR spectrometer at 400 MHz (or 300 MHz) for $^1H$ and 100.6 MHz (or 75.4 MHz) for $^{13}C$ in $CDCl_3$ using TMS as the internal standard. The electron paramagnetic resonance method for data acquisition was previously described.[5a] Gas chromatography was performed on a HP 5890 gas chromatograph equipped with a FID detector and a HP-1 capillary column. GC/MS was performed on a HP 5890II gas chromatograph equipped with a HP-5 capillary column and connected to a HP 5972 Mass Selective Detector. Scanning electron microscopy (SEM) was performed on a Hitachi S-510 scanning electron microscope.

**2,2,6,6-Tetramethyl-4-[(phenylacetyl)oxy]-1-piperidinyloxy, (1). 1** was synthesized on the basis of a modified published procedure.[6] To a solution of phenylacetic acid (2.85 g, 20.9 mmol), 4-hydroxy-TEMPO (3 g, 17.4 mmol) and 4-pyrrolidinopyridine (0.31 g, 2.09 mmol) in 50 mL dry ether was added 1,3-dicyclohexylcarbodiimide (DCC) (5.03 g, 24.4 mmol) in 10 mL dry ether. The reaction mixture was stirred for 24 h under an argon atmosphere, diluted with a mixture of 100 mL water and 100 mL methylene chloride, and then stirred for 5 min. After filtering off the precipitate, the organic layer was collected and washed in sequence with an aqueous solution of 2 × 100 mL 0.5 N HCl, 3 × 100 mL 1 N NaOH, and 2 × 100 mL water, 100 mL of saturated NaCl aqueous solution and dried over anhydrous magnesium sulfate. The crude product was concentrated at reduced pressure and was purified by flash column chromatography. Elution was achieved with hexanes/ethyl acetate/methylene chloride with increasing polarity from 20:1:1 (volume) to 14:1:1, and was monitored by thin-layer chromatography visualized by UV (254 nm) and an iodine chamber. After removal of the solvent under reduced pressure, 3.6 g of **1** (12.4 mmol) as red viscous oil was obtained in 71% yield. The sample used in the EPR experiment was at least 95% pure, as confirmed by GC analysis. MS (EI) (rel intensity): 290 (6.5), 154 (18), 119 (56), 104 (55), 91 (100).

**2,2,6,6-Tetramethyl-4-[(2-methylphenylacetyl)oxy]-1-piperidinyloxy, (1-oMe). 1**-oM**e** was prepared following the procedure described above for **1** using 2-methylphenylacetic acid instead of phenylacetic acid. The product was obtained as a viscous red oil after purification by column chromatography.

**1,3-Bis(2-methylphenyl)-2-propanone, (2). 2** was synthesized following a published procedure for the synthesis of 1,3-

bis(4-methylphenyl)-2-propanone using 2-(methylphenyl) acetic acid instead of 4-(methylphenyl) acetic acid.[7] **2** was purified by column chromatography with hexanes/ether (19/1 v/v) and was re-crystallized from hexanes/ether as white crystals. $^1$H NMR (ppm) 7.13−7.22 (3H, m), 7.06−7.09 (2H, m), 3.73 (4H, s), 2.17 (6H, s). $^{13}$C NMR (ppm) 205.9, 137.1, 133.1, 130.7, 130.6, 127.6, 126.4, 47.5, 19.8.

**1,2-Bis(2-methylphenyl)ethane, (3). 3** was isolated from the reaction mixture in the preparation of **4** (vide infra) as a side product and re-crystallized as white crystals. $^1$H NMR (ppm) 7.14−7.26 (8H, m), 2.85 (4H, s), 2.32 (6H, s). $^{13}$C NMR (ppm) 140.3, 136.1, 130.4, 129.0, 126.3, 126.2, 34.3, 19.5.

**1-(2-Methylphenyl)-3-phenyl-2-propanone, (4). 4** was synthesized following a published procedure for the synthesis of 1-(4-methylphenyl)-3-phenyl-2-propanone using 2-(methylphenyl) acetic acid instead of 4-(methylphenyl) acetic acid.[7] It was purified by column chromatography with hexanes/ether (19/1 v/v) and obtained as a colorless liquid at room temperature. $^1$H NMR (ppm) 7.26−7.35 (3H, m), 7.11−7.21 (5H, m), 7.02−7.11 (1H, m), 3.74 (2H, s), 3.71 (2H, s), 2.13 (3H, s). $^{13}$C NMR (ppm) 205.9, 137.2, 134.2, 133.0, 130.6, 128.9, 127.6, 127.2, 126.4, 49.3, 47.5, 19.7.

**Zeolites.** Silicalite (Si/Al > 1000) was obtained from UOP. LZ-105, a pentasil, ZSM-5 type zeolite (Na form, Si/Al = 20) was a generous gift from Dr. Edith Flanigen of Union Carbide Corporation. The mean crystal size of the silicalite was ca. 1 $\mu$m and the mean crystal size of the LZ-105 sample was ca. 0.3 $\mu$m (SEM characterization). The external surface areas of silicalite (5 m$^2$/g) and a LZ-105 (16 m$^2$/g) were determined using mercury porosimetry.[5a,8]

**Sample Preparation.** The zeolite samples were activated in a furnace at 500 °C for 2 h and cooled to room temperature in a desiccator prior to use.

A typical sample preparation of the EPR probes adsorbed on the zeolites was as follows: a stock solution of 10 mg of **1** (or **1**-oMe) in 10 mL of isooctane was prepared. For loading less than 0.3%, the desired amount of stock solution was diluted to 0.3 mL and mixed with 100 mg of zeolite. For loading higher than 0.3%, an appropriate amount of stock solution (more than 0.3 mL) was mixed with 100 mg of zeolite. The slurry was then stirred for 30 min. The loading is expressed in weight percent throughout this paper, i.e., 1% corresponds to 1 mg of adsorbate on 100 mg of zeolite.

A typical sample preparation of the EPR probes with coadsorbed molecules was as follows: stock solutions of 10 mg of **1** (or **1**-oMe) in 10 mL of isooctane and of 10 mg of the **2**, **3**, and **4** in 10 mL of isooctane were prepared. A specific loading was achieved by mixing appropriate volumes of stock solutions of **1** (or **1**-oMe) and the coadsorbed molecule with isooctane to form 0.3 mL of solution. Then, 100 mg of the zeolite were added to the mixture and stirred for 30 min.

For all the samples, after stirring, the solvent was removed first by evaporation with an argon flow and then under vacuum to $1 \times 10^{-4}$ Torr.

**Computation of the EPR Spectra.** The EPR spectra were computed by means of the procedure established by Schneider and Freed.[9] For each series of measurements (different loading for the same zeolite) the following parameters were calculated for the spectrum at the lowest loading in the series and then assumed constant for the other spectra of the series:

(1) $g_{ii}$ (components of the **g** tensor for the magnetic field−electron spin coupling):

$g_{ii}$ = 2.009, 2.006, 2.002 for silicalite samples, and $g_{ii}$ = 2.009, 2.006, 2.0025 for LZ105 samples.

The error limit in the $g$ value is $\pm 5 \times 10^{-5}$ as obtained from the calculation as follows: The computed line shape significantly changes only for values above and below the indicated accuracy.

(2) $A_{ii}$ (components of the **A** tensor for the electron spin-nuclear spin coupling):

$A_{ii}$ = 6 G, 7 G, 38 G for all samples; the high $A_{ii}$ values indicate a very polar environment of the radical situated at the zeolite surface. The error limit in the calculation of $A_{ii}$ is 2% as obtained from calculation, as above for the $g$ values.

(3) $\tau$ (correlation time for the rotational motion of the radical, e.g., the mean value between the parallel and the perpendicular component whose ratio was assumed constant = 10). The calculation of this parameter from the computation procedure was obtained assuming a Brownian model for the rotational motion of the nitroxide.[9]

The error limit of $\tau$ is estimated to be ±2.5% as obtained from the calculation [$\tau$ values larger than the ones above (+2.5%) or smaller than those above (−2.5%) produced a significant variation in the computed line shape, decreasing the goodness of fitting between the experimental and the computed signals].

When the radicals begin to interact strongly with each other (spin−spin interactions) either statically due to their vicinity or dynamically through collisions of mobile radicals, the sensitivity of the calculation to the polarity and motion parameters diminishes. However, at this point the parameters connected to spin−spin interactions become important in the spectral simulation and can be employed to obtain information on the supramolecular structure and dynamics of the adsorbed radicals, rather than on the polarity and motion.

The following parameters were used for the computation of spin−spin interactions that occur at high loadings of the nitroxides:

(1) $\Delta H_D$, the dipolar broadening that is included in the intrinsic line width in the calculation.[10] The evaluation of the dipolar broadening (due to static anisotropic spin−spin interactions) by means of spectral computation, allows the calculation of the mean distance, $d$ (in Å, among the probes at the surface, from the equation, $\Delta H_D = 3 \times 10^4/d^3$.[11] The error limit in the line width from spectral simulation and in the calculated $d$ is estimated to be ca. ±2.5%. In the calculation the interacting spins are assumed fixed with respect to each other. This would be the situation for radicals associated with the holes on the external surface.

(2) $\omega_{ex}$, Heisenberg spin−spin exchange frequency.[12] The increase in $\omega_{ex}$ also corresponds to the increase in the local concentration of the mobile radicals whose motion allows collision with other nitroxides on the external surface. The error limit in $\omega_{ex}$ is estimated to be ca. ±2.5% as obtained from spectral simulation.

For some spectra, the fitting between the experimental and computed spectra was not as good as others, due to both the approximations assumed for the parameters in the calculation and the assumption that only one component (and, therefore, one set of parameters) contributes to the EPR signal. It may be that the radicals are bound in more than one environment even at low loadings or that different supramolecular stereoisomers may contribute to the binding at either site.[13b] However, for the purposes of the present study, the parameters extracted from computation are sufficient to provide information on the evolution of the system as a function of loading (absolute values are not required for the qualitative analysis).

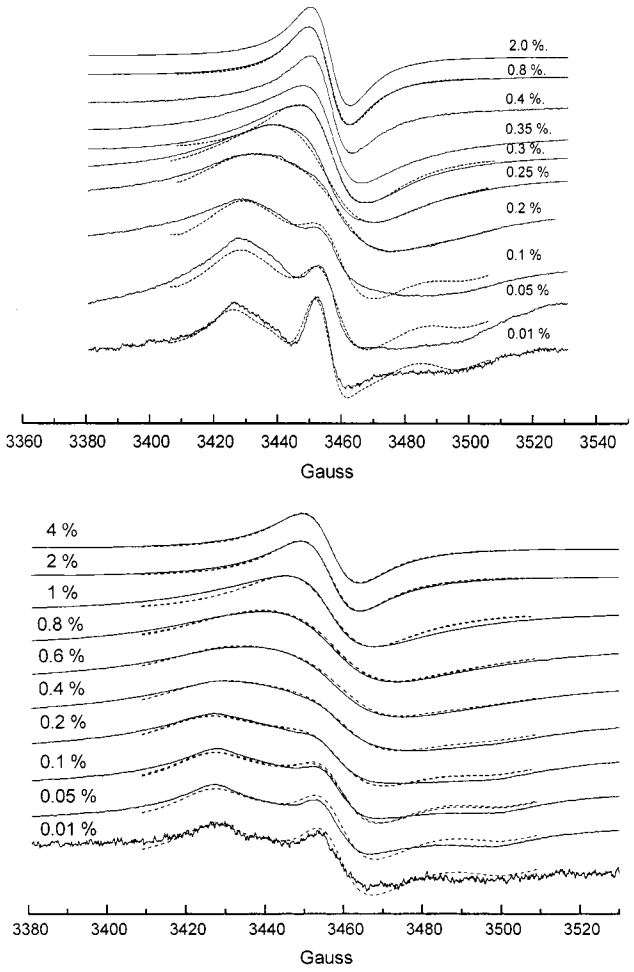


**Figure 1.** (a) EPR spectra of **1** on silicalite at various loadings, indicated at the right of the spectra. The solid lines are experimental results and the dashed lines are from computational simulations. (b) EPR spectra of **1** on LZ-105 at various loadings, indicated at the left of the spectra. The solid lines are experimental results and the dashed lines are from computational simulations.

## Results and Discussion

Figure 1 shows the EPR experimental spectra (solid lines) and computed spectra (dashed lines) of **1** adsorbed at different loading onto silicalite (Figure 1a) and LZ-105 (Figure 1b).

The computation of the spectra at the lowest loading allowed for an evaluation of the correlation times for motion as: $\tau = 7 \times 10^{-9}$ s for silicalite samples, and $\tau = 1 \times 10^{-8}$ s for LZ-105 samples.

It is to be noted that these times are in the so-called slow motion limit of the EPR method ($(1-2) \times 10^{-9}$ s $< \tau < 5 \times 10^{-8}$ s).[9] These results at low loading (0.01−0.05%) of **1** (or **1**-oMe, not shown) are consistent with the proposed model which predicts that the initial adsorption of **1** will be associated with the stronger binding sites of the external surface. In addition to the holes as "pores" for intercalation of a portion of the probe, portions of the probe structure can interact with polar groups such as SiOH groups[13,4d4] (silicalite and LZ-105) and cations [13,4d4] (LZ-105) that exist on the external surface. The slower mobility of **1** on the LZ-105 surface relative to the silicalite surface is consistent with a higher polarity and the presence of cations on the surface near the holes for LZ-105. It is also possible that some portion of the nitroxide probe partially inserts itself into the holes on the external surface and is stabilized by dispersion interactions.

The assumption that the EPR parameters are constant at low and high loading is only an approximation, since the environment and supramolecular structure of the radicals@zeolite are expected to change with loading. The radicals' size and shape prevent them from being adsorbed into the internal surface. They bind first to the holes and then to the framework between the holes. The initial binding to the holes causes the EPR spectra to be dominated by the dipolar interaction between nitroxides at fixed positions in the holes on the external zeolite surface. As the loading increases, the holes are eventually saturated with nitroxides. Beyond the saturation loading, the framework between the holes serve as binding sites for **1** until a monolayer is formed. In this case, the dynamic exchange interaction results from the interactions of weakly adsorbed mobile radicals on the framework of the external surface which are relatively free to diffuse and collide with each other and with the constrained radicals associated with the holes. The onset of mobile nitroxides on the framework may set up a dynamic equilibrium between the stronger and weaker binding sites. If radicals associated with the holes are displaced by dynamic equilibrium, the dipolar interactions between these radicals will be averaged out and will "disappear" from the EPR signals.

Although information on static dipolar interactions and average distances of separation disappears at high loading, new information on the dynamics of exchange of radicals between sites becomes available, because the radicals that undergo rapid collisions at high concentration give rise to Heisenberg exchange interaction (the electron spins exchange among radicals) which can be extracted by computational EPR analysis of the spectra. The exchange frequency increases with the increase of loading on the framework and is manifested by a collapse of the hyperfine lines into a single line. Therefore, the lowest loading corresponding to the onset of the exchange interaction provides an indication of the saturation of nitroxide molecules associated with the holes and the onset of the coverage of the framework of the external surface by the nitroxide when the spins of the radicals can interact statically due to their proximity or dynamically due to their weaker binding to the framework.

Loadings beyond a monolayer causes the formation of a nitroxide multilayer at the surface in which the radicals are mainly surrounded by other radicals creating a fluid two-dimensional film of low-polarity.

The $\Delta H_D$ and $\omega_{ex}$ parameters obtained from computational analysis of the EPR spectra are listed in Table 1 for the spectra of **1**-oMe reported in Figure 1. From the parameters in Table 1, the sum of the spin-narrowed spectra (a single line due to the collapse of the hyperfine lines) may easily be computed by means of at least two sets of parameters. For instance, from 0.25% to 0.3% loading on silicalite we tried to either retain the same line width or to decrease the line width, in both cases increasing the exchange frequency to reproduce the EPR line shapes. The physical meaning of these two choices is of course very different, a decrease in dipolar line width with increasing loading being much more probable, due to interactions of the nitroxides in the holes with mobile colliding nitroxides.

**EPR Analysis of the Loading Dependence of Adsorption of 1 and 1-oMe on Silicalite and LZ-105.** The results of the computational EPR analysis were experimentally indistinguishable for the loading dependence of adsorption of **1** and **1**-oMe on either silicalite or LZ-105. Thus, the structural and dynamic interpretation will be the same for each probe so that only the results for **1** will be discussed in detail. Despite the possibility of the occurrence of heterogeneity of binding, it is

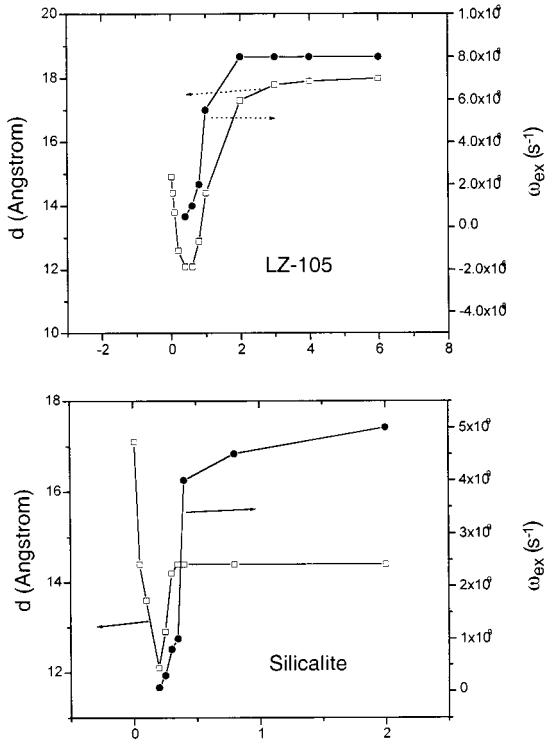


**Figure 2.** Mean distance (*d*, Å, left ordinate) and Heisenberg spin−spin exchange frequency ($\omega_{ex}$, right ordinate) between probe molecules **1** derived from computational analysis of EPR spectra of Figure 1 at different loadings on the external surface of LZ-105 (top) and silicalite (bottom).

**TABLE 1: Parameters for the Spin−Spin Interactions As Obtained from Computational Analysis of the EPR Spectra of 1 onto Silicalite and LZ-105**

| zeolite | loading (wt/wt %) | $\Delta H_D$ (Gauss) | $\omega_{ex}$ (s) |
|---|---|---|---|
| silicalite | 0.01 | 6 | |
| | 0.05 | 10 | |
| | 0.1 | 12 | |
| | 0.2 | 17 | $7 \times 10^7$ |
| | 0.25 | 14 | $3 \times 10^8$ |
| | 0.3 | 14 | $1.5 \times 10^9$ |
| | | 10−10.5 | $8 \times 10^8$ |
| | 0.35 | 10 | $1 \times 10^9$ |
| | 0.4 | 10 | $4 \times 10^9$ |
| | 0.8 | 10 | $4.5 \times 10^9$ |
| | 2 | 10 | $5 \times 10^9$ |
| LZ-105 | 0.01 | 9 | |
| | 0.05 | 10 | |
| | 0.1 | 11.5 | |
| | 0.2 | 15 | |
| | 0.4 | 17 | $5 \times 10^7$ |
| | 0.6 | 17 | $1 \times 10^8$ |
| " | 0.8 | 17 | $3 \times 10^9$ |
| | | 14 | $2 \times 10^8$ |
| | 1 | 17 | $3 \times 10^9$ |
| | | 10 | $5.5 \times 10^8$ |
| | 2 | 10 | $2 \times 10^9$ |
| | | 5.8 | $8 \times 10^8$ |
| | 3−4 | 10 | $2.5 \times 10^9$ |
| | | 5.3 | $8 \times 10^8$ |
| | 6 | 10 | $3.5 \times 10^9$ |
| | | 5.1 | $8 \times 10^8$ |

clear (Figure 2) that the *d* value (average separation between probe nitroxides in Å, left ordinate) decreases almost linearly for loadings up to 0.2%, an indication that the radicals are initially adsorbed and are immobile at interacting sites that are separated by a fixed distance from each other. The variation in slope above ca. 0.2% for LZ-105 is due to the progressive saturation of proximal sites, that is, the surface holes. At ca. 0.2% loading for silicalite and ca. 0.4% loading for LZ-105, the radical−radical distance reaches a minimum value (ca. 12 Å) and the exchange frequency begins contributing and must be taken into account in the calculation. As discussed above, we may take the onset of spin−spin interactions to indicate the saturation of the surface sites (holes) to which the nitroxide molecules adsorb. The saturation value for filling the holes by **1** on silicalite (ca. 0.2%) is in good agreement with the saturation value (ca. 0.2%) obtained from a spectroscopic and photochemical analysis of **4** adsorbed on silicalite.[5a] The difference in the saturation values between the two zeolites (ca. 0.2% for silicalite and ca. 0.4% for LZ-105) is the result of the differences in the surface areas of the two zeolites, which are ca. 5 $m^2/g$ for the silicalite sample and about 16 $m^2/g$ for the LZ-105 sample.

An important check of the computation is provided by a comparison of the minimum values of *d* (ca. 12 Å) from Figure 2. This computed value compares favorably with that derived from X-ray data for the minimum distance between the centers of two adjacent holes (ca. 12 Å). The excellent agreement between the value of *d* from X-ray data and EPR computation provides support for the validity of the assumption that saturation corresponds to filling the holes on the external surface and that binding to the holes is sufficiently strong to immobilize the probes on the EPR time scale.

Beyond the saturation point, (>0.2% for silicalite and >0.4% for LZ-105), the plots in Figure 2 (both a dynamic spin−spin exchange and "formal" distance of separation of the probes) may be computed from the spectra. The result is an almost linear *increase* in *both* the distance among the radicals and the exchange frequency. Although the increase in exchange frequency is intuitively expected because of the increase in the number density of the probes as the surface coverage increases and the corresponding increase in collisions between surface bound molecules, the *increase* in separation between probes is in apparent contradiction to an increase in surface coverage and requires an explanation.

The apparent contradiction between the results of the dipolar interactions and the exchange interactions (Figure 2) can be explained on the basis of the following model for adsorption of the probe on the external surface (Chart 3). The model assumes that the initial strong binding site (holes, Chart 3a) "fixes" or "freezes" the motion of the probe (on the EPR time scale) at a certain average distance, *d*, which decreases with increasing coverage and population of the holes. Eventually, the holes are all filled (saturation, Chart 2b) and the average distance between the probes bound to the holes is at a minimum. Beyond saturation, further binding must occur at the second site (framework) which does not constrain the motion of the probe significantly. The diffusional motion of the probes adsorbed on the framework will result in collisions with other probe molecules, both those bound to the holes and to the framework. Both types of collisions will result in an increased frequency of dynamic spin−spin exchange ($\omega_{ex}$). However, collisions between a mobile probe bound to the framework and a fixed probe bound to a hole provides a mechanism for dynamic displacement of the probe in the hole (Chart 3c). In effect, the onset of adsorption of probe molecules on the framework provides a dynamic mechanism for removing probes from the hole and for establishing an equilibrium between probe molecules in both sites. Since the total amount of external surface

**CHART 3: Schematic Representation of the Adsorption of Nitroxide 1 onto the External Surface of Silicalite at Various Loadings[a]**

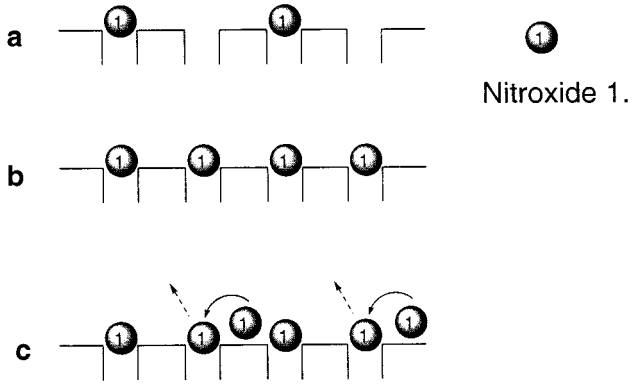


[a] (a) At low loading, **1** strongly binds to the holes, the stronger binding site. The average distance between "fixed" molecules of **1** decreases with increasing loading as the holes are filled to produce a partial coverage of the external surface. (b) When the holes are saturated, the lowest *d* value is observed. (c) At higher loading, molecules of **1** begin binding to the framework at the external surface. the latter are mobile and a dynamic exchange between the molecules occurs. See text for discussion.

**CHART 4: Schematic Representation of Nitroxide 1 (0.01%) on External Surface of MFI Zeolite with Coadsorbed 2, 3, 4 as Displacers of 1 from Holes[a]**

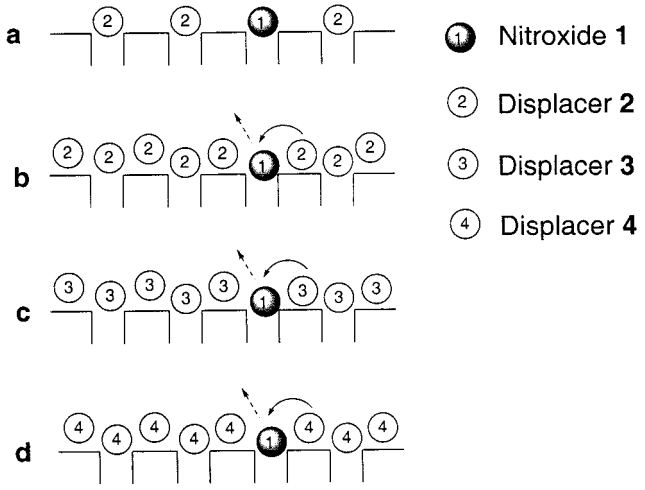


[a] (a) **2** binds strongly to the holes of external surface along with a small coverage of **1** until saturation of the holes is achieved without effect on the binding of **1**; (b) **2** begins adsorbing on the framework of the external surface and mobile molecules of **2** begin colliding with and displacing **1** from the holes; (c) at loading up to a monolayer, molecules of **3** do not interact strongly with the external surface of MFI zeolite and fail to displace **1**; (d) molecules of **4** do not bind as strongly as **1**, so they will only start displacing **1** after filling in all the remaining holes and occupying, at least partially, the framework between the holes.

is finite, when the external surface is completely covered, the rate of the dynamic exchange of sites reaches a maximum.

The proposed dynamic mechanism for displacement from the holes, which is absent until the framework becomes covered, is an interesting property of adsorption on surfaces. The mechanism operates when there are two binding sites that are limited in number and for which the first site binds much more strongly than the second site. If the activation for removal (and subsequent diffusion) from the first site is high (on the EPR time scale) and determined by a unimolecular process, the EPR analysis shows the probes as fixed until the sites are saturated. After saturation, further addition of mobile probes provides a second order mechanism for removal of the probe from the more strongly binding sites. The contribution of the second-order displacement process increases as the concentration of the mobile probes (adsorbed on the framework) increases.

This model provides a means of rationalizing the intuitively unexpected increase in the computed average distance between EPR probes as the coverage increases beyond the saturation point of the holes. The model predicts that the lifetime of the association of a nitroxide with a hole or framework decreases as the result of site exchange. The dynamic displacement of radicals associated with holes and the resulting motion averages the dipolar interactions between some of the fixed radicals associated with holes, causing them to become "invisible" to other fixed radicals in holes in the computation of *d*. As a result, the distance between the radicals associated with holes appears to *increase* as the coverage increases beyond saturation because of the removal of dipolar interactions, which the computation interprets as an increase in the average separation between the probes in the holes.

As is expected from the model, beyond a certain loading corresponding to complete coverage of the external surface (at ca. 2% for silicalite and ca. 4% for LZ-105), the average distance and the exchange frequency remain almost constant (Figure 2). At this point there is a complete coverage of the external surface and the formation of a "fluid monolayer", a situation for which there is a rapid exchange of nitroxide at all sites. The final value of the exchange frequency is higher on silicalite (ca. $5 \times 10^9$ $s^{-1}$) than on LZ-105 (ca. $8 \times 10^8$ $s^{-1}$) and is attributed to the smaller surface area of the silicalite samples.

As mentioned above, the results for **1**-oMe closely parallel those of **1** within the experimental uncertainty. Thus, the phenyl group of **1** is probably not bound strongly to the holes of the external surface by intercalation, since this mode of binding is not likely for **1**-oMe; i.e., the molecular cross section of the "*o*-xylene" portion of **1**-oMe is too large to fit in the holes of the external surface. We conclude that, since the stronger binding site for **1** is stoichiometrically correlated with the holes on the external surface, there must be some *chemical* feature of the holes that is important in the binding. This feature could be the occurrence of "defects" (e.g., SiOH groups) for silicalite and of SiOH or such groups and cations for LZ-105. With this qualification in mind, for convenience and simplicity we shall continue to refer to the stronger binding sites as those associated with the holes, and the weaker binding site as those associated with the framework.

**Dependence of the EPR of 1 Adsorbed on Silicalite and LZ-105 on Loading of Coadsorbed 2, 3, and 4.** Having established that the EPR spectra of adsorbed nitroxide provide a probe of binding and of dynamic nitroxide exchange of sites on the external surface, we now employ EPR to examine the ability of a series of "displacer" molecules (**2**, **3**, and **4**) to replace nitroxide molecules associated with the holes (i.e., low loading of **1**). Chart 4 shows schematically some of the supramolecular structures and dynamics that are expected to be formed by the coadsorption of **1** and **2**−**4**. It is expected that as **1** is displaced from association with holes by coadsorbed **2**, **3**, or **4**, the EPR of the adsorbed nitroxide will be converted from one characteristic of a bound probe in slow motion to one of a freely moving probe in fast motion. The displacer molecules were selected to provide different structural features that would result in differing binding and displacing abilities. Ketone **2** possesses a polar carbonyl group and two nonpolar aryl moieties,

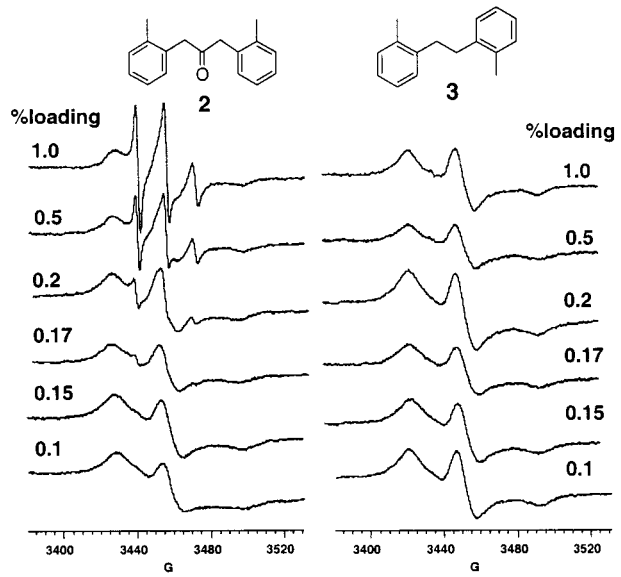


**Figure 3.** EPR spectra of **1** (0.01%) on external surface of silicalite at various loadings of coadsorbed **2** and **3**.

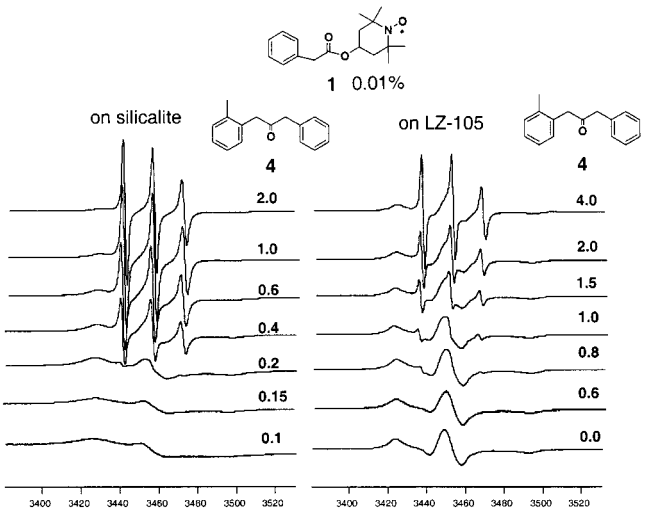


**Figure 4.** EPR spectra of **1** (0.01%) on external surface of silicalite (left) and LZ-105 (right) at various loadings of coadsorbed **4**.

neither of which can intercalate into a hole on the external surface. Hydrocarbon **3** possesses a nonpolar structure that cannot intercalate into a hole on the external surface, but can be weakly bound to the framework. Ketone **4** possesses a polar carbonyl group and two nonpolar aryl rings, one of which can intercalate into the holes on the external surface.

If the molecules **2**, **3**, and **4** displace **1** from the holes to the framework, the EPR spectrum of **1** will transform from one that is characteristic of the probe in slow motion (broad, wide line spectrum) to one that is characteristic of the probe in fast motion (sharp, three-line spectrum). Figure 3 shows the experimental EPR spectra obtained upon coadsorption of various amounts of **2** and **3** onto silicalite together with 0.01% of **1**. At the latter low loading, in the absence of coadsorbates, **1** is associated with the holes on the external surface and displays an EPR spectrum characteristic of a probe in slow motion (Figure 3, bottom spectra). The spectrum of **1** coadsorbed with **2** does not change with increased loading until reaching the loading corresponding to saturation of the holes (ca. 0.2%) of the external surface (shown schematically, Chart 4a). This loading value is in excellent agreement with the value for saturation loading of the holes deduced from the loading dependence of the EPR of **1** alone (Figure 2).[5a] Above this loading value, a signal due to fast moving radicals (three narrow lines) begins contributing to the EPR spectra (shown schematically in Chart 4b). As the loading increases from this point on, the contribution of the sharp three-line spectrum increases in relative intensity with the increase in loading of **2**.

Therefore, it is concluded that the ketone progressively binds to the holes until saturation occurs and then begins to bind to the external frameworks. At this point a dynamic exchange model employed to describe the displacement of nitroxide by ketone molecules between sites becomes important and the nitroxide is displaced from association with the holes as the result of collisions with **2** bound to the framework. Because of the large excess of **2** as the loading increases, the nitroxide becomes increasingly displaced to the external framework and the condition of rapid motion is achieved. At very high loadings (>2%) a fluidlike monolayer is formed and exchange among sites becomes very rapid.

The results with **3** as a nitroxide displacer are quantitatively different from those for **2** (note the onset of the sharp spectrum at ca. 0.2% for **2** and the absence of any hint of the sharp spectrum for this loading for **3**). Even at high loading of **3** (>1%), only a small fraction of **1** is displaced (shown schematically in Chart 4c) from the fixed positions (holes), whereas a significant fraction of **1** is displaced at this loading by **2**. The main structural difference between **2** and **3** is the occurrence of a polar C═O group for **2**, whereas **3** is nonpolar. The differing behavior of **2** and **3** provides information on the chemical nature of the external surface of the silicalite samples. As discussed above, there must be polar "defects", such as SiOH groups, on the external surface of the silicalite and the number of these polar sites are associated with and evidently scale in number as the number of holes on the external surface. Since **1** has two polar functional groups (ester and nitroxide) associated with its structure, it will bind strongly to the polar groups associated with the holes on the silicalite surface. Since nonpolar **3** only weakly interacts with the zeolite surface, it does not compete effectively with **1** for the polar binding sites (holes) on the external surface. Thus, collisions between **3** adsorbed on the framework and the nitroxide molecules associated with the holes are ineffective in displacing the nitroxides, at least up to 1% loading.

Note that the sharp EPR lines for the fast moving radicals cannot be observed in the case of adsorption of pure **1** on silicalite (or LZ-105), because spin−spin interactions gave rise to the collapse of the hyperfine EPR lines well before saturation of the holes occurs. Thus, the indirect EPR method (increasing loading of ketones with a small and constant amount of **1**) can be seen to complement the direct EPR method (increasing loading of pure **1**) for analysis of binding of **1** to the zeolite surface.

Figure 4 shows the EPR spectra of **1** at 0.01% loading onto the silicalite and LZ-105 with different loadings of coadsorbed ketone **4**. This ketone possesses a partial structure that mimics **1** more closely than the structure of ketone **2**, since the phenyl moiety of both **1** and **4** may intercalate into the holes on the external surface, but the aryl moiety of **2** cannot. As in the case of **2,** the free component in the EPR signal does not appear until near or after the saturation of the holes is reached (Chart 4 d). This saturation condition is ca. 0.2% of **4** for the silicalite samples and is consistent with the EPR analysis of adsorbed **1** without coadsorbed **4** as described above. However, the saturation for LZ-105 occurs at higher loading percentage (ca. 1% of **4**) with respect to that found for the nitroxide by EPR without

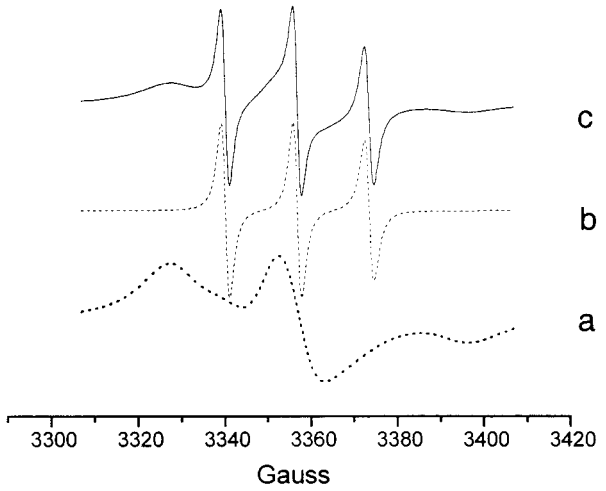


**Figure 5.** Addition of EPR spectra at slow motion and fast motion to reproduce an experimental spectrum. (a) spectrum computed for slow motion, (b) spectrum computed for fast motion. (c) result from addition of (a)and (b), to produce a good fit to the experimental spectrum.

coadsorbed **4** and shown in Figure 2 (minimum of *d* at 0.4% of **1**).[14] This discrepancy may arise from the different affinity of **1** and **4** toward the more polar LZ-105 surface. Both structures are expected to anchor at the surface holes through intercalation of the phenyl group, but the nitroxide possesses two polar sites, whereas **4** only possesses one. The LZ-105 external surface is more polar than the silicalite external surface due to the high cation content and binds more strongly to the polar moieties. Therefore, the ketone and nitroxide molecules may lie on the surface more easily and interact with the surface through their polar groups. The lower spin−spin interaction and the lower mobility of **1** adsorbed at the LZ-105 surface, in contrast to silicalite, are consistent with this proposal.

Above saturation, the amount of radicals removed from the surface holes upon collisions and competition with the ketone molecules progressively increases. By comparing the various samples, the results can be summarized as follows: (a) The amount of **1** being displaced at the silicalite surface by means of collisions with the displacer molecules at high loading (ca. 1%) increases in the series: **3** < **2** < **4**, the minimum being for the highly hydrophobic **3** and the maximum for **4,** the closer structural analogue of the nitroxide **1**; (b) In comparing the 0.6% sample of silicalite to the 4% sample of LZ-105, the discrepancy in the saturation point between silicalite and LZ-105 is even higher at higher loading with respect to low loading. This indicates that it is necessary to have a very large amount of ketone to displace the nitroxide at the LZ-105 surface and that the nitroxide is more strongly bound to this surface relative to **4**.

In general, the sequence of addition (nitroxide first, ketone second, or vice-versa) did not have a significant effect on the visual appearance of the EPR spectra obtained. Possible effects of the order of addition were investigated by quantitative investigation of the amount of the free nitroxide component. Computation of the spectra was made by computing both the free and slow signals and adding the two components at the right ratio to reproduce the experimental line shape. Figure 5 provides an example of such a computation. For silicalite it was found that there is a small discrepancy between the plots of the fraction of free component obtained by first loading of the ketone or the radical or by mixing both together (data not shown). However, the percentage of the fast component increased to a lesser degree when the radical **1** was added before the ketone **4**, as compared to the opposite addition sequence. This is to be expected, since the radical molecules will have all the zeolite holes available for the interaction if added prior to the ketone. The small discrepancy among these plots confirms the fact that the affinity of the radical toward the surface is higher than the affinity of the ketone, expected on the basis of the relatively high polarity of the nitroxide radical in contrast to the ketone, and is consistent with the conclusions given above. Also it is interesting to note that the amount of free component was found to increase almost linearly with the increase of loading, providing evidence for the equivalence of the strongly binding sites (holes) at the zeolite surface.

## Conclusions

EPR analysis has been employed to investigate the loading dependence of the supramolecular structures and dynamics of nitroxide probes adsorbed on MFI zeolites (silicalite and LZ-105) in the presence and absence of "displacer" molecules (**2**, **3**, and **4**). Mobility and structural parameters were extracted by computer-aided analysis of the EPR spectra. At low loading of **1**, mobility and separation parameters of the probe nitroxide were extracted form the dipolar interactions between nitroxides. At high loading of **1,** spin−spin interactions had to be included in spectral calculation, and motion parameters were extracted from the spin exchange interactions between nitroxides. The EPR analysis reveals that at low loading, nitroxide molecules first associate with and eventually saturate the holes on the external surface and that the interaction responsible for binding are mainly between the polar groups of the nitroxide and the polar surface sites (e.g., SiOH groups for silicalite and SiOH and cations for LZ-105). Weaker interactions may result from partial intercalation of the phenyl groups and/or the nitroxide groups into the hole. After saturation of the holes, the external framework is occupied by weakly bound molecules, eventually forming a monolayer on the external surface. Collisions between fixed (in the holes) and mobile (framework) nitroxides (a) increased the average distance among the fixed molecules as obtained by the dipolar broadening of the EPR lines; (b) increased the Heisenberg exchange frequency of the colliding radicals; and (c) caused dynamic displacement of the radicals from the holes. The model employed to rationalize the results for the dependence of the EPR of **1** alone on loading is sufficient to explain the dependence of the EPR of **1** on variation of the loading of coadsorbed **2**, **3**, and **4**.

The following conclusions are reached concerning the competitive binding among the **1**−**4** molecules: (a) interaction with the surface is favored for **1** relative to **2**, **3**, and **4** due to the presence of two polar groups which can attach to the external surface; (b) competition to replace **1** from the fixed surface sites (holes) increases in the series: **3** < **2** < **4**, the minimum being for the nonpolar **3** and the maximum for **4**, the closer analogue of the nitroxide **1**. Comparison between the results from the two zeolites (silicalite and LZ-105) indicated that the different amounts of adsorption of the ketones is affected by the different external surface areas, with the LZ-105 external surface area being 2−3 times larger than the silicalite area. In addition, adsorption is strongly influenced by the different polarity of the surfaces which favor a different orientation of molecules with respect to the surface: the more polar LZ-105 surface preferentially accepts the polar moieties so that ketone and nitroxide molecules may lie on the surface more easily and interact with the surface. The model in Chart 4 summarizes these results: **2** and **4** are able to displace the radicals from the surface holes at relatively low loadings, whereas **3** displaces nitroxide molecules associated with holes only at high loading.

**Acknowledgment.** The authors at Columbia thank the National Science Foundation for its generous support of this work under Grant No. NSF CHE-98-12676. This work was supported in part by a grant to the Environmental Molecular Sciences Institute (EMSI) at Columbia by the Department of Energy and the National Science Foundation (NSF CHE-98-103672). M.F.O. thanks the Italian Ministero Universita e Ricerca Scientifica (MURST) for financial support. The authors thank Dr. Lloyd Abrams of the Central Research & Development Department of the DuPont Corporation for many insightful comments and for assistance in measuring the external surface areas. The authors thank Mr. Timothy Biegeleisen of Cornell University who participated in the NSF supported summer REU program at Columbia University and participated in the synthesis of **1**-oMe. The authors thank Mr. Rokan Ahmao in Prof. Richard Osgood's research group at Columbia University for performing the SEM measurements.

## References and Notes

(1) (a) Csicsery, S. M. *Zeolite Chemistry and Catalysis*; Rabo, J. A., Ed; ACS Monograph No. 171; American Chemical Society: Washington, DC, 1976; Chapter 12. (b) Derouane, E. G. *Zeolites: Science and Technology*; Ribeiro, F. R., Ed.; Nijhoff: Boston, 1984; p 347. (c) Derouane, E. G.; Gabilica, Z. *J. Catal*. **1980**, *65*, 486. (d) *Diffusion and Shape Selective Catalysis in Zeolites*; Derouane, E. G., Ed.; Academic Press: New York, 1982.

(2) (a) Brecker, D. W. *Zeolite Molecular Sieves: Structure, Chemistry and Use*; John Wiley & Sons: New York, 1974; p 373. (b) Argauer, R. J.; Landolt, G. R. U.S. Pat. 3,702,886, 1972. (c) Meier, W. M.; Olson, D. H. *Atlas of Zeolite Structure Type*s, 2nd rev. ed; Butterworth: London, 1987; pp 100−101.

(3) (a) Weisz, P. B. *Ind. Eng. Chem. Fundam*. **1986**, *25*, 53. (b) Csicsery, S. M. In *Zeolite Chemistry and Catalysis*; Rabo, J. A., Ed; ACS Symposium Series 171; American Chemical Society: Washington, DC, 1976; p 680. (c) Derouane, E. G. in *Intercalation Chemistry*; Whittingham, M. S., Jacobson, A. J. Eds.; Academic Press: New York, 1982; p 101. (d) Derouane, E. G. *Catalysis by Zeolites*; Imelik, B., Ed.; Elsevier: Amsterdam, 1980; p 5.

(4) (a) For a selection of IR, Raman, UV diffuse reflectance, and NMR spectroscopy, see Ramamurthy, V. Photoprocesses of Organic Molecules Included in Zeolites. In *Photochemistry in Organized and Constrained Media*; Ramamurthy, V., Ed; VCH Publishers: New York, 1991; Chapter 10. (b) For a recent review on Raman spectroscopy, see Knops-Gerrits, P. P.; De Vos, D. E.; Feijen, E. J. P.; Jacobs, P. A. *Microporous Mater*. **1997**, *8*, 3. (c) For recent progress in IR spectroscopy (picosecond IR laser spectroscopy), see Bonn, M.; Bakker, J. H.; Kleyn, A. W.; Van Santen, R. A. *Appl. Surf. Sci*. **1997**, *121*, 80; for FTIR and diffuse-reflectance IR spectroscopy, see *Top. Catal*. **1997**, *4*, 131. (d) For additional literature on NMR spectroscopy, see the following: Dybowski, C. *J. Inclusion Phenom. Mol. Recognit. Chem*. **1995**, *21* (1−4), 113; Klinowski, J. *Prog. Nucl. Magn. Reson. Spectrosc*. **1984**, *16* (3−4), 237; Eckman, R. R.; Vega, A. J. *J. Phys. Chem*. **1986**, *90*, 4679; and Pfeifer, H.; Meiler, W.; Deininger, D. NMR of Organic Compounds Adsorbed on Porous Solids. In *Annual Reports on NMR Spectroscopy*; G. A. Webb, Ed.; Academic Press: London, 1983, Vol. 15, pp 291−356, and references therein. (e) For X-ray photoelectron spectroscopy, see Borade, R.; Sayari, A.; Adnot, A.; Kaliaguine, S. *J. Phys. Chem*. **1990**, *94*, 5989. (f) For EPR spectroscopy see Eastman, M. P.; Gonzalez, J. A. *J. Phys. Chem*. **1985**, *89*, 488; Rigo, A.; Viglino, P.; Ranieri, G.; Orsega, E. F.; Sotgiu, A. *Inorg. Chim. Acta* **1977**, *21* (1), 81. (g) For fluorescence spectroscopy, see Iu, K.-K.; Thomas, J. K. *Langmuir* **1990**, *6*, 471; Incavo, J. A.; Dutta, P. K. *J. Phys. Chem*. **1990**, *94*, 3057; Ramamurthy, V.; Eaton, D. F.; Caspar, J. V. *Acc. Chem. Res*. **1992**, *25*, 299; Liu, X.; Thomas, J. K. *Langmuir* **1993**, *9*, 727; Cozens, F. L.; Regimbald, M.; Garcia, H.; Scaiano, J. C. *J. Phys. Chem*. **1996**, *100*, 18165.

(5) (a) Turro, N. J.; Lei, X.-G.; Li, W.; Liu, Z.; McDermott, A.; Ottaviani, M. F.; Abrams, L. *J. Am. Chem. Soc*. **2000**, *122*, 11649. (b) Hirano, T.; Li, W.; Abrams, L.; Krusic, P. J.; Ottaviani, M. F.; Turro, N. J. *J. Org. Chem*. **2000**, *65*, 1319. (c) Turro, N. J.; Lei, X.-G.; Li, W.; Liu, Z.; Ottaviani, M. F. *J. Am. Chem. Soc*. **2000**, *122*, 12571. (d) Turro, N. J. *Acc. Chem. Res*. **2000**, *33*, 637. (e) Li, W. Ph.D. Dissertation, Columbia University, 1999.

(6) (a) Hassner, A.; Alexanian, V. *Tetrahedron Lett*. **1978**, *46*, 4475. (b) Hassner, A.; Krepski, L. R.; Alexanian, V. *Tetrahedron* **1978**, *34*, 2069.

(7) Turro, N. J.; Weed, G. C. *J. Am. Chem. Soc*. **1983**, *105*, 1861.

(8) Abrams, L.; Keane, M.; Sonnichsen, G. C. *J. Catal*. **1989**, *115*, 410.

(9) Schneider, D. J.; Freed, J. H. In *Biological Magnetic Resonance. Spin Labeling. Theory and Applications*; Berliner, L. J., Reuben, J., Eds.; Plenum Press: New York, 1989; Vol. 8.

(10) (a) Plachy, W.; Kivelson, D. J. *Chem. Phys*. **1967**, *47*, 3312. (b) Aikaawa, M.; Komatsu, T.; Nakagawa, T. *Bull. Chem. Soc. Jpn*. **1979**, *52*, 980; *ibid*. **1980**, *53*, 975.

(11) Sackmann, E.; Traeuble, T. *J. Am. Chem. Soc*. **1972**, *94*, 4482, 4492, 4499.

(12) Hyde, J. S.; Swartz, H. M.; Antholine, W. E. In *Spin Labeling. Theory and Applications*; Berliner, L. J., Ed.; Academic Press: New York, 1979; Vol. 2, p 71.

(13) (a) Jackson, K. T.; Howe, R. F. In *Surface Science, Principles and Current Applications*; MacDonald, R. J., Taglauer, E. C., Wandelt, K. R., Eds.; Springer: Berlin, 1996; p 331. (b) Turro, N. J.; Lei, X.-G.; Niu, S.; Liu, Z.; Jockusch, S.; Ottaviani, M. F. *Org. Lett*. **2000**, *2*, 3991. (c) Kubelkova, L.; Cejka, J.; Novakova, J. *Zeolites* **1991**, *11*, 48.

(14) Expressed in molar units, the ratio of loading of **4** to **1** corresponding to the wt/wt percent of loading indicated is 2.5:1.